THE FLUID MECHANICS OF FORWARD DIRECT GRAVURE COATING

Hadj Benkreira[1] and Olivier Cohu

Dpt. of Chemical Engineering, University of Bradford, West Yorkshire BD7 1DP, U.K.

ABSTRACT

This experimental study of forward gravure coating considers the effects of operating variables on air entrainment, ribbing instabilities and the thickness of the film formed. The data show that this coating method can yield very thin films of thickness of order of 15 - 20% at most of the equivalent cell depth of a gravure roller. Air free and non ribbed stable uniform films can however only be obtained in a narrow window of operating conditions at very low substrate capillary number (Ca_S ~ 0.02) equivalent to substrate speeds typically less than 20m/min. The paper draws a similarity with flow features observed with smooth forward roll coating and slide coating. It is shown that the onset of ribbing and the flux distribution between the gravure roller and the substrate at the exit of the nip obey approximately the same rules as in smooth forward roll coating, whereas the onset of air entrainment actually corresponds to a low-flow limit of coatability similar to that observed in slide coating.

Keywords : Coating, Gravure, Print, Flow Instabilities, Film Thickness, Experiments

1 - INTRODUCTION

Coating flows are fluid flows which result in thin films of liquid forming onto surfaces and are engineered for the manufacture of a variety of products. Typical examples include paper and adhesive tapes, photographic and X-ray films, magnetic tapes for audio, video and computer use, electronic circuit boards, printing plates for papers, books and magazines and coated papers for printing (Cohen and Gutoff, 1992). The terminology associated with coating methods is diverse but they can all be classified according to Benkreira *et al.* (1994) into one or a combination of the following broad ways:

(1) *free coating* such as in the unhindered withdrawal of liquid from a pool by a moving substrate;

(2) *metered coating* such as when an excess amount of liquid is metered in a flow geometry to form a film onto a moving substrate (*e.g.* blade, air knife, forward or reverse roll coating);

(3) *transfer coating* where an exact amount of liquid is delivered in a flow geometry to form a film onto a moving substrate (kiss, die, slot, slide or curtain coating);

(4) *print or gravure coating* where a film is formed when a moving substrate wipes a proportion of a coating trapped in the cells of a printed or gravure roller.

[1] corresponding author: Tel (01274) 383721 Fax (01274) 385700 Email H.Benkreira@bradford.ac.uk

None of these flows can operate to yield the wide range of film thicknesses (5-500 microns) and speeds (0.1- 25 m/s) required in practice without exhibiting non uniformity (instabilities) on the free surface in the form of ribs or air bubbles entrained in the film. For each coating flow there is a narrow stable window of operation, not always easily predictable. The stability windows observed with reverse roll coating (Coyle *et al.*, 1990a) and slot coating (Sartor, 1990) are typical examples. As we move down these types of flows to gravure coating, thinner films (5-15 microns) can be attained (in principle as low as we can engrave the cells) but the onset of instabilities limit the speed of application and the conditions at which these occur are not yet known.

Whereas types (1), (2) and (3) flows have been well researched theoretically and experimentally and significant progress has been made in their understanding (for a review, see Kistler and Schweitzer, 1997), research in type (4) flow – *print or gravure coating* – is very limited (Pulkrabek and Munter, 1983 ; Patel and Benkreira, 1991 ; Benkreira and Patel, 1993) and this may be attributed to the complexity of the geometry of the flow system. Print or gravure coating uses a roller with a pattern of cells of regular and precise geometry which are either chemically or mechanically engraved on it. These cells form complex patterns (see fig. 1) such as the quadrangular, trihelical and pyramidal geometries with cell volume per unit area of about 5 to 50 x 10^{-6} m^3/m^2 and a wetted area coverage of 0.80 to 0.90 m^2/m^2 of roller surface. In actual operations, the engraved cells are flooded with the coating liquid and the excess which forms over is wiped by a blade pressed against the rotating roller. The liquid trapped in the cells is then transferred onto the substrate usually in one of three ways as illustrated in fig. 2 : direct forward, direct reverse or indirect forward known also as offset gravure when the substrate is arranged in "kiss contact" with the impression roller (*i.e.* not sandwiched between the gravure and impression rollers). In the classification adopted above, the offset mode is not a key coating flow *per se*; it is composed of a *gravure* coating flow and a *transfer* coating flow. Also, flow situations where a surplus film is formed over the cells are strictly not gravure coating flows which are designed, as explained above, specifically with the aim of achieving the thinnest possible films. The blade loading over the gravure roller forms thus an important part and this aspect was investigated by Patel and Benkreira (1991) who showed experimentally that higher cell volume factors reduce the surplus film but that true gravure coating is not easily achieved unless very low viscosity fluids are used. The practical difficulty of completely doctoring the surplus, without excessively loading the blade hence possibly damaging the cells particularly with standard chromed rollers, can explain the use of an impression rubber roller instead of a doctor blade to remove the surplus liquid at entry to the nip. It is also thought that this arrangement controls the thickness of the final film formed and the onset of ribbing instabilities and air entrainment. These observations are *known* in industrial practice but no underlying studies are available to underpin and quantify these effects.

The transfer of the liquid from the cells to the moving substrate in the direct reverse mode of operation was studied experimentally by Benkreira and Patel (1993) and their findings indicate that about 1/3 of the cell volume is transferred as a film at large speeds regardless of speed ratios (between the moving web and gravure roller). At low speeds, there appears to be a maximum in the film thickness curves for the trihelical and pyramidal cell configurations suggesting that larger films are formed *i.e.* the cells which are deeper empty better at low speeds. The reverse was observed with the quadrangular geometry where the cells are shallower and a minimum occurs at low speeds.

At present no comprehensive studies of the other two modes of gravure coating operations have been made. The aim of this investigation is to extend our knowledge of gravure coating flows by looking at applications when the gravure roller and the substrate move in the same direction at the nip with no impression roller (direct forward mode). Measurements of the film thickness variations with operating conditions and the determination of the ribbing instability and air entrainmemt limits are the objectives of this experimental investigation. Another objective is to draw analogies with other coating flows to explain the key features of the fluid mechanics of forward direct gravure coating.

2 - EXPERIMENTAL METHODS

The experimental work was carried out on a pilot coater described schematically in fig. 3. It consists essentially of a stainless steel frame with spring loaded bearing blocks which hold the rollers perfectly horizontally by adjusting the dial microgauges on each side of the rollers shaft. The rollers and substrate (a 25 microns Melinex film) were independently driven. Three gravure rollers, a 220 quadrangular, a 85 trihelical and a 60 pyramidal (the number refers to the number of cells per inch) with cell volume per unit area of roller surface V_c of 13.25, 28.50 and 43.37 x 10^{-6} m^3/m^2 respectively were used. These geometries, described in fig. 1, were established using the Taylor Hobson replica method (essentially a means of obtaining a plastic duplicate of the surface which could be sliced into microns size cross sections and photographed under a microscope) and the Talysurf method (essentially a means of measuring a surface profile using a precision diamond tipped stylus attached to a pivoting arm which can travel along the surface). All the rollers were 0.182 m wide and their diameter D was 0.1 m. In the direct mode of operation, an additional variable is the wrap angle θ_W of the substrate round the gravure roller. To assess this effect, four wrap angles, 0, 4.0, 10.0 and 14.5 degrees were tested. The applied web tension was monitored using an air operated unit (the Mount Hope total tension indicator system) which indicated the average web tension of the moving web as it travelled over a load sensing idler roller. In all the experiments the web tension was maintained at 450 N/m and the thickness h_S of the film formed on the substrate was measured using an infra-red thickness gauge suitably calibrated and accurate to +/-0.5 microns. The onset of air entrainment and ribbing, was assessed visually under good lighting conditions, using repeat experiments. In the study six water based Newtonian solutions were tried and their viscosities, μ, and surface tensions, σ, were in the range 1 - 14 x 10^{-3} Pa.s and 30 - 67 x 10^{-3} N/m respectively as measured using the Brabender Rheotron viscometer and the drop-weight method. Table 1 shows the range of the experimental conditions used. In keeping with the application of gravure coating, high viscosity fluids were not tested as they generate high hydrodynamic loads beneath the doctor blade and this violates the essential condition for true gravure that a surplus film must not form over the cells (Patel and Benkreira, 1991).

3 - AIR ENTRAINMENT AND RIBBING INSTABILITIES

The first set of experiments was designed to establish broadly the stability window (onset of air entrainmement and/or ribbing) and study its features. U_G and U_S being the speeds of the gravure roller and the substrate, respectively, experiments were carried out at a constant speed ratio $S \equiv U_G / U_S$ from 0.5 to 1.5 in steps of 0.25 for U_S varying from 10 to 40 m/min (well

into the unstable regime) in steps of 10 m/min. From the results obtained, a second set of experiments was designed to draw more precisely the envelope of the stability window. Substrate speeds of 5, 7.5, 10 and 20 m/mn were used and the gravure roller speed was increased from 10 to 100 m/mn in steps of 10 m/mn. In total, with four wrap angles, six liquids and three gravure geometries, about 1100 data points were recorded.

When the substrate speed was higher than the gravure roller speed (*i.e.* $U_S > U_G$), air entrainment in the form of evenly spaced lines of fine bubbles always developed in the machine direction. To avoid it at a given U_G, U_S had to be decreased considerably in comparison, until the limit of air entrainment, U_{SA} was reached. At that point, an increase of the gravure roller speed prevented air entrainment and the operation was stable. Further increases of U_G however, led, at a critical U_{GR}, to the appearance of ribbing instabilities. Ribbing manifested itself as in other coating flows with evenly spaced uniform down-web lines ondulating the surface of the coating. For a given combination of liquid, gravure roller and wrap angle, plotting the data obtained as in fig. 4, in terms of the gravure roller speed U_G against the substrate speed U_S shows the map of the stable window to be bounded by a low air entrainment curve and a high ribbing instability curve. The low curve steepens as the substrate speed increases and a maximum coating speed was found above which air entrainment always occured. On the top right part of the curve, air entrainment and ribbing occured together. The results shown in fig. 4 are typical of all the data obtained. As detailed below, they may be interpreted as the combination of the classical ribbing instability window observed with smooth forward roll coating (Pitts and Greiller, 1961 ; Benkreira *et al*, 1982 ; Coyle *et al*., 1990b) and the transition from stable flow to air entrainment and / or rivulet flow displayed by transfer coating (slide coating for example) and often refered to as the low-flow limit of coatability (Gutoff and Kendrick, 1987).

As for the mechanisms, the ribbing instability must be linked to the formation of a meniscus and films on the substrate and the gravure roller on exit from the nip. The picture is very similar to smooth forward roll coating. In smooth forward roll coating, the onset of ribbing depends on the gap over diameter ratio and on the average capillary number $Ca_m \equiv \mu [U_G + U_S] / 2\sigma$ (Benkreira *et al*, 1982 ; Coyle, 1992). In gravure coating no gap is preset between the roller and the substrate but an appropriate dimension is the equivalent cell depth V_c. Thus, if we plot the data obtained with a single gravure roller but different liquids in terms of the gravure roller capillary number $Ca_G \equiv \mu U_G / \sigma$ against the substrate capillary number $Ca_S \equiv \mu U_S / \sigma$, a master curve for the ribbing instability should be obtained. This is shown in fig. 5 with a zero wrap angle. For comparison purposes, we have also plotted in fig. 5 the straight lines $Ca_m = Ca^*$, where Ca* is the capillary number for the onset of ribbing in symmetric forward roll coating computed by Coyle *et al.* (1990b) as a function of the gap over diameter ratio (which here must be taken as $V_c / 2D$ in the roll and plate configuration). Calculated values of Ca* for the three gravure geometries are reported in table 2. It should be emphasised that comparing our results with Ca* presents some risks since this presupposes that the onset of ribbing does not depend on the speed ratio. Indeed it can be seen that the stable domain in fig. 5 can hardly be bounded by a straight line of slope -1 (that is of constant *average* capillary number). Rigourously speaking, the onset of ribbing in our experiments did not depend on the *average* capillary number Ca_m but rather on Ca_S and Ca_G independently, which in fact is in agreement with the recent experimental findings of Decré *et al.* (1996). Irrespective of such details, it can be seen in fig. 5 that in forward gravure high capillary numbers and low V_c favour ribbing altogether, as it is the case when smooth rollers are

considered. However, the results show that the V_c gap constitutes only a crude approximation for the prediction of the onset of ribbing. As a general rule, gravure roll coating is more prone to ribbing than expected from the data of smooth roll coating with the V_c gap. This is particularly obvious with the 220 quadrangular geometry, for which no stable coating could be obtained. Conversely, the analogy with smooth roll coating is fairly good with the 85 trihelical geometry. These results suggest that the *shape* of the individual cells of the gravure roller also plays a role in the ribbing instability and that at constant V_c the trihelical geometry must be the most stable one. Further experiments using gravure rollers having the same volume factor V_c but different cell geometries would be useful to confirm this hypothesis.

On the other hand, the flow situation in gravure coating resemble that encounterred in transfer coating processes since a controllable flow rate that can be expressed here as $Q = U_G V_c$ is delivered to the substrate. Transfer coating flows such as slide coating are subject to limits beyond which uniform coating cannot be achieved and the coating breaks down into evenly spaced rivulets and / or air is entrained (Gutoff and Kendrick, 1987). At a given flow rate, the coating speed cannot be increased above a critical speed. Similarly, at a given substrate speed, the flow rate cannot be decreased below a critical value. These two limits are actually one and the same and are known as the low-flow limit of coatability. For a given liquid, there is also a maximum speed above which stable coating is impossible regardless of the flow rate. All these trends can be observed from the data obtained with regard to air entrainment in gravure roll coating. The fact that air entrainment manifested itself as evenly spaced lines of fine bubbles rather than in an erratic manner supports the analogy with the low-flow limit of coatablity in slide coating. Moreover, plotting the data obtained with the three gravure geometries and different liquids in terms of the flow rate $Q = U_G V_c$ as a function of the substrate capillary number Ca_S results in a mastercurve showing the low-flow limit of coatability of gravure coating. This is shown in fig. 6 with zero wrap angle. The range of film thicknesses (or flow rates) and capillary numbers involved in gravure roll coating are very different than those in slide coating, so that a quantitative comparison of the low-flow limits of coatability in both flow situations is not possible. Nevertheless, drawing the analogy between gravure and slide coating is very instructive. As in slide coating, high substrate speeds and high viscosity liquids favour air entrainment. On the other hand, air entrainment is cleared by increasing the flow rate supplied to the substrate, and this explains why air entrainment is cleared by *increasing* the speed of the gravure roller. For the same reason, gravure rollers having a large volume factor V_c are less prone to air entrainment. Conversely, the results indicate that the shape of the individual cells of the gravure roller is at most a second order parameter with regard to the air entrainment problem, since the data obtained for the three gravure geometries fall on the same mastercurve as shown in fig. 6.

In conclusion, the complex stability window in forward gravure roll coating can be understood using the double analogy of gravure roll coating with smooth roll coating and transfer coating methods. Not surprisingly, high substrate speeds and high viscosity liquids, or equivalently high substrate capillary numbers Ca_S, favour both ribbing and air entrainment. As a result, stable coating operations could not be run at substrate capillary numbers Ca_S above 10^{-2} (with zero wrap angle). The role of the speed of the gravure roller U_G is more complex. High U_G retard air entrainment by increasing the flow rate supplied to the substrate, but also favour ribbing by increasing Ca_G and hence the average capillary number Ca_m. For a given gravure geometry and a given liquid, the speed of the gravure roller hence the film thickness that can be applied at a given substrate speed (see next section) is then bounded by a minimum and a maximum. On the other hand, low values of the cell volume factor V_c

favour both ribbing and air entrainment. As a result, uniform coating could not be possibly achieved using the 220 quadrangular gravure roller of small $V_c = 13$ μm. The results also suggest that an optimum design of the shape of the cells of the gravure roller would have no effect on air entrainment but could slightly stabilise the flow with regard to ribbing.

An additional variable as mentioned earlier is the wrap angle of the substrate around the gravure roller. The data presented in fig. 7 show that as the wrap angle was increased the stability window widened, with both air entrainment and ribbing onsets retarded to higher speeds. For instance, it was found that for a given gravure roller capillary number Ca_G a wrap angle greater than 10° could increase by 50 to 100 % the maximum substrate capillary number Ca_S at which stable coating operation was possible. These trends are consistent with similar observations reported in both forward roll coating and transfer coating. When the wrap angle is not zero, the tension of the web results in a load that pushes the substrate against the gravure roller, and the system becomes elastohydrodynamic. The stability of the elastohydrodynamic flow between a smooth roller and a tensioned web is very little documented in the open literature. However, Carvalho and Scriven (1996) showed that the onset of ribbing in a two-roll coater is delayed when deformable rolls are used, which suggests that elastohydrodynamic roll coating systems in general are less prone to ribbing. Similarly, elastohydrodynamic transfer coating systems such as tensioned-web slot coating are less subject to air entrainment (Pranck and Coyle, 1997), as the extra pressure arising from the web tension *via* the wrap angle assists dynamic wetting. Therefore, the stabilising effect of the wrap angle in gravure roll coating can be explained. An immediate outcome of this analysis is that when the wrap angle differs from zero the stability window must also depend on the web tension and on the elastic properties of the substrate. The analysis also suggests that the use of an impression rubber roller (see fig. 2) also widens the stability window, which was actually observed during preliminary experiments reported elsewhere (Benkreira *et al.*, 1996).

4 - TRANSFERED FILM THICKNESS

As explained above, instabilities limited the speed of coating in all cases to less than 20 m/mn equivalent to $Ca_S \sim 0.02$. Moreover, for a given substrate speed within that range, the speed of the gravure roller was also bounded so that in practical terms the speed ratio $S \equiv U_G / U_S$ must be between, say, 3 and 8 (see Benkreira *et al.*, 1996). The coating window can be even narrower or even does not exist, as with the 220 quadrangular geometry and no wrap angle. Nevertheless, in order to understand the mechanisms that determine the final coating thickness, it is worth including in the analysis the data for which air entrainment and / or ribbing were observed, as this widens considerably the range of parameters that can be investigated.

We found no effect of the substrate wrap angle on the coating thickness. The thickness h_S of the film deposited onto the substrate results from (1) the total flow rate which is supplied by the gravure roller to the coating nip, $Q = U_G V_c$, and (2) the film-splitting flow that occurs at the exit of the nip, as part of the liquid remains trapped in the cells of the gravure roller while the remainder is transfered onto the substrate. The results show that this film-splitting flow may be described as a base flow similar to the film-splitting flow in smooth forward roll coating, with a perturbation due to the presence of a gravure roller. It has been established

both experimentally (Benkreira *et al.*, 1981) and theoretically (Coyle *et al.*, 1986) that the film-splitting flow of a Newtonian liquid between two smooth counterrotating rollers moving at speeds U_S and U_G follows

$$Q_G / Q_S = (U_G / U_S)^{1.65} \quad , \tag{1}$$

where Q_G and Q_S are the flow rates (film thickness × speed) carried by the rollers at the exit of the nip. Transposed to the gravure coating situation, with $Q = Q_S + Q_G = U_G V_c$, eq. (1) expressing the flux distribution can be rewritten as

$$S (V_c / h_S) - 1 = S^{1.65} \quad . \tag{2}$$

Eq. (2) was tested against experimental data as shown in fig. 8. In spite of a significant scattering, the cause of which is discussed later, the data in the log-log plot follow the theoretical slope of 1.65 fairly well, which confirms the similarity of film-splitting flows in smooth and gravure forward roll coating. However, the experimental data appear to be shifted from the theoretical curve as they are best fitted by

$$S (V_c / h_S) - 1 = \beta S^{1.65} \quad , \tag{3}$$

where β is an asymmetry factor experimentally comprise roughly between 2 and 3. That β is greater than unity expresses the fact that more liquid than predicted by eq. (1) remains in the cells of the gravure roller, *i.e.* that the gravure pattern hinders the transfer of the liquid onto the substrate. Seen like this, β may depend on the gravure geometry though this does not appear clearly in fig. 8 due to the scattering of the data.

In gravure coating operations, the dimensionless coating thickness, *i.e.* the ratio of the coating thickness to the cell volume factor of the gravure roller, is of practical interest. Eq. (3) leads to a simple expression of h_S / V_c ,

$$h_S / V_c = S / (\beta S^{1.65} + 1) \quad , \tag{4}$$

which shows that for a typical speed ratio of 5 the dimensionless film thickness is less than 1/6. This value is half that measured by Benkreira and Patel (1993) in reverse gravure coating which was always about 1/3 independently of the speed ratio. In other words, forward gravure coating is capable to produce significantly thinner films than the reverse situation. This is namely because forward gravure involves a film-splitting flow where the dimensionless film thickness is strongly dependent on the speed ratio. It is interesting to note that with a speed ratio of 1 the dimensionless film thickness is practically the same whether the operation is conducted in the forward or in the reverse mode, as with $S = 1$ eq. (4) gives h_S / V_c comprised between 1/3 and 1/4.

As mentioned earlier, a significant scattering may be observed in fig. 8 where the experimental data of the flux distribution are plotted against the speed ratio only. This is due to the fact that the pick-up of the liquid from the cells of the gravure roller also depends on the *global* hydrodynamic forces developed in the nip by the liquid, that is on the *average* capillary number Ca_m. This is shown in fig. 9 where the dimensionless coating thickness is

plotted against Ca_m for two values of the speed ratio S. As explained above, increasing the speed ratio decreases the dimensionless film thickness. Moreover, it is clear from fig. 9 that regardless of the gravure geometry increasing the average capillary number at constant speed ratio increases the dimensionless film thickness. This shows that *global* viscous forces (expressed by Ca_m) help to pull the liquid out the cells so that at high Ca_m the dimensionless film thickness gets closer to its corresponding value in smooth forward roll coating.

In summary, the dimensionless film thickness in forward gravure coating is a quite complex function of the operating parameters as it is determined *independently* by (1) the speed of the gravure roller which sets the flow rate supplied to the nip to the coating nip, (2) the speed ratio which governs the film-splitting base flow as in forward roll coating, and (3) the average capillary number (hence the average speed) that controls how perturbed is the film-splitting base flow compared to the smooth roll coating case. The dimensionless film thickness may also depend on the shape of the individual cells of the gravure roller but this effect could not be assessed from our experimental results.

5 - CONCLUSION

This investigation shows that direct forward gravure coating produces very thin films of thickness 15 - 20% at most of the equivalent cell depth compared to the 33% produced by reverse gravure. This process is also more flexible as it was shown that the film thickness depends on operating parameters such as substrate and roller speeds, which is not the case in the reverse mode of operation. These performances are related namely to the fact that forward gravure coating flow involves a film-splitting flow as in forward roll coating, whereas the flow situation in reverse gravure resembles more that observed in kiss coating where the liquid film carried by the applicator roller is wiped off by the substrate.

However, it was shown that unloaded forward gravure coating combines the air entrainment and ribbing instabilities observed with slide coating and smooth forward roll coating respectively. These features result in a rather complex and very narrow coating window. In particular uniform and air-free films can be applied only at low substrate speeds nominally less than 20 m/min which limits the scope of applications. It was observed that gravure rollers with high cell volume factor are less prone to instabilities. Wrapping of the substrate round the roller also help stabilising the flow without altering the film thickness.

ACKNOWLEGEMENTS

The support of the ERASMUS European exchange student scheme which enabled J.M. Leclercq of the Faculte Polytechnique de Mons, Belgium to carry out most of the experimental work, is gratefully acknowledged. The authors are indebted to Dr R. Patel for his constant help throughout this programme of research. Thanks are also due to E. Jones for her assistance in the processing of the experimental data. Dr O. Cohu is supported by a grant awarded by the Commission of European Communities under the Training and Mobility of Researchers Programme.

LIST OF SYMBOLS

Ca_G	Gravure roller capillary number $Ca_G \equiv \mu U_G / \sigma$	-
Ca_S	Substrate capillary number $Ca_S \equiv \mu U_S / \sigma$	-
Ca_m	Average capillary number $Ca_m \equiv [Ca_S + Ca_G] / 2$	-
Ca*	Theoretical value of Ca_m at the onset of ribbing in forward roll coating (S = 1)	-
D	Roller diameter	m
h_S	Coating thickness	m
Q	Flow rate supplied to the nip by the gravure roller (per unit width)	m^2/s
Q_G	Flow rate remaining on the applicator (gravure) roller (per unit width)	m^2/s
Q_S	Flow rate transfered onto the substrate (per unit width)	m^2/s
S	Speed ratio U_G / U_S	-
U_G	Gravure roller speed	m/s
U_S	Substrate speed	m/s
U_{GR}	Gravure roller speed at the onset of ribbing	m/s
U_{SA}	Substrate speed at the onset of air entrainment	m/s
V_c	Cell volume per unit area of roller surface (equivalent cell depth)	m
β	Asymmetry factor of the film-splitting flow	-
μ	Fluid viscosity	Pa.s
σ	Fluid surface tension	N/m
θ_W	Wrap angle of the substrate round the gravure roller	^{o}

REFERENCES

Benkreira, H., Edwards, M.F., and Wilkinson, W.L. (1981) "Roll Coating of Purely Viscous Liquids", *Chem. Eng. Sci.* **36**, 429

Benkreira, H., Edwards, M.F., and Wilkinson, W.L. (1982) "Ribbing Instability in the Roll Coating of Newtonian Liquids", *Plastics Rubber Proc. Appl.*, **2**, 137

Benkreira, H., and Patel, R. (1993) "Direct Gravure Roll Coating", *Chem. Eng. Sci.*, **48**, 2329

Benkreira, H., Patel, R., Edwards, M.F., and Wilkinson, W.L. (1994) "Classification and Analyses of Coating Flows", *J. Non-Newt. Fluid Mech.*, **54,** 437

Benkreira, H., Patel, R., Naheem, M., and Leclercq, J.M. (1996) "Film Thickness and Instabilities with Forward Gravure Coating" *in* "The Mechanics of Thin Film Coating", P.H. Gaskell, M.D. Savage, and J.L. Summers Eds., World Scientific, Singapore, pp 213-220

Carvalho, M.S., and Scriven, L.E. (1996) "Deformable Roll Coating : Analysis of Ribbing Instability and its Decay" *in* "The Mechanics of Thin Film Coating", P.H. Gaskell, M.D. Savage, and J.L. Summers Eds., World Scientific, Singapore, pp 75-84

Cohen, E., and Gutoff, E.B., Eds. (1992) “Modern Coating and Drying Technology”, VCH Publishers, New York

Coyle, D.J. (1992) “Roll Coating”, *in* “Modern Coating and Drying Technology”, E. Cohen and E.B. Gutoff Eds., VCH Publishers, New York, pp 63-116

Coyle, D.J., Macosko, C.W., and Scriven, L.E. (1986) “Film-Splitting Flows in Forward Roll Coating”, *J. Fluid Mech.*, **171**, 183

Coyle, D.J., Macosko, C.W., and Scriven, L.E. (1990a) “The Fluid Dynamics of Reverse Roll Coating”, *AIChE J.*, **36**, 161

Coyle, D.J., Macosko, C.W., and Scriven, L.E. (1990b) “Stability of Symmetric Film-Splitting Between Counter-Rotating Cylinders”, *J. Fluid Mech.*, **216**, 437

Decré, M., Buchlin, J.M., Schmidt, J., and Rabaud, M. (1996) “The Onset of Ribbing Reconsidered : an Experiment” *in* “The Mechanics of Thin Film Coating”, P.H. Gaskell, M.D. Savage, and J.L. Summers Eds., World Scientific, Singapore, pp 387-396

Gutoff, E.B., and Kendrick, C.E. (1987) “Low Flow Limits of Coatability on a Slide Coater”, *AIChE J.*, **33**, 141

Kistler, S.F., and Schweitzer, P.M., Eds. (1997) “Liquid Film Coating : Scientific Principles and their Technological Implications”, Chapman & Hall, London

Patel, R., and Benkreira, H. (1991) “Gravure Roll Coating of Newtonian Fluids”, *Chem. Eng. Sci.*, **46**, 751

Pitts, E., and Greiller, J. (1961) “The Flow of Thin Liquid Films Between Rollers”, *J. Fluid Mech.*, **11**, 33

Pranckh, F.R., and Coyle, D.J. (1997) “Elastohydrodynamic Coating Systems”, *in* “Liquid Film Coating : Scientific Principles and their Technological Implications”, S.F. Kistler and P.M. Schweitzer Eds., Chapman & Hall, London, pp 599-636

Pulkrabek, W.W., and Munter, J.D. (1983) “Knurl Roll Design for Stable Rotogravure coating”, *Chem. Eng. Sci.*, **38**, 1309

Sartor, L. (1990) “Slot Coating : Fluid Mechanics and Die Design”, PhD thesis, University of Minnesota, Minneapolis

Legends of Figures and Tables
(9 figs. - 2 tables)

Fig. 1 Gravure geometries

Fig. 2 Gravure coating flows

Fig. 3 Experimental pilot coater

Fig. 4 Typical coating window in forward gravure coating. Gravure roller 60 pyramidal ; zero wrap angle ; $\mu = 1.036$ mPa.s ; $\sigma = 30$ mN/m ; Δ stable coating ; ● air entrainment ; ■ ribbing

Fig. 5 Ribbing limit of the coating window in gravure roller capillary number *vs* substrate capillary number diagram. All liquids ; zero wrap angle ; gravure rollers : ☐ pyramidal, Δ trihelical, ✧ quadrangular ; white symbols : stable coating ; black symbols : ribbing ; ------ onset of ribbing in smooth forward roll coating with V_c gap

Fig. 6 Air entrainment limit of the coating window in flow-rate *vs* substrate capillary number diagram. All liquids; zero wrap angle; gravure rollers : ☐ pyramidal, Δ trihelical, ✧ quadrangular ; white symbols : stable coating ; black symbols : air entrainment

Fig. 7 Effect of the wrap angle on the coating window. Gravure roller 85 trihelical ; $\mu = 1.403$ mPa. ; $\sigma = 30$ mN/m ; upper plot : zero wrap angle ; lower plot : 10º wrap angle ; Δ stable coating ; ● air entrainment ; ■ ribbing

Fig. 8 Film-split ratio *versus* speed ratio. All liquids ; zero wrap angle ; gravure rollers : ☐ pyramidal, Δ trihelical, ✧ quadrangular ; ——— smooth roll coating

Fig. 9 Dimensionless film thickness *versus* average capillary number for speed ratio of 1 (white symbols) and 10 (black symbols) ; all liquids ; zero wrap angle ; gravure rollers : ☐ pyramidal, Δ trihelical, ✧ quadrangular

Table 1 : Ranges of parameters investigated

Table 2 : Critical capillary numbers in symmetric smooth roll coating (roll and plate configuration) calculated with the V_c gaps corresponding to the three gravure geometries (from Coyle *et al.*, 1990b)

Parameter		Range			Unit
Gravure Roller Speed	U_G	5	-	100	m/mn
Substrate speed	U_S	10	-	40	m/mn
Cell Volume Factor	V_c	13.25	-	43.37	μm
Fluid Viscosity	μ	1.036	-	14.06	mPa.s
Fluid Surface Tension	σ	30	-	67	mN/m
Wrap Angle	θ_W	0	-	14.5	°

Table 1

(D = 0.1 m)	V_c / 2D	Ca*
60 Pyramidal	2.16×10^{-4}	4.0×10^{-2}
85 Trihelical	1.43×10^{-4}	3.3×10^{-2}
220 Quadrangular	6.63×10^{-5}	2.3×10^{-2}

Table 2

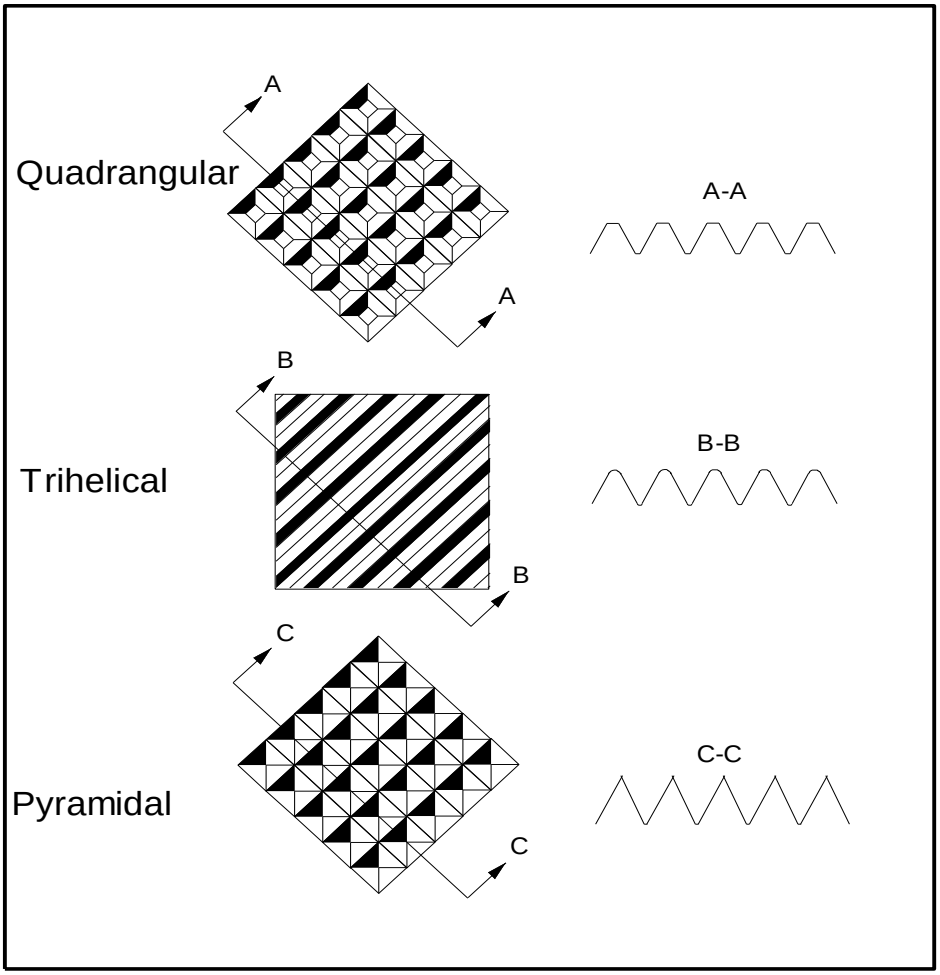

Fig. 1

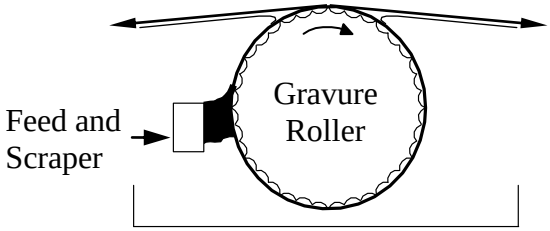

Direct, forward or reverse
on unsupported web

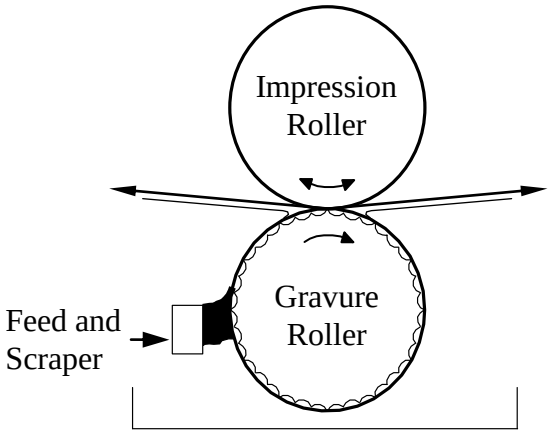

Direct, forward or reverse
with impression roller

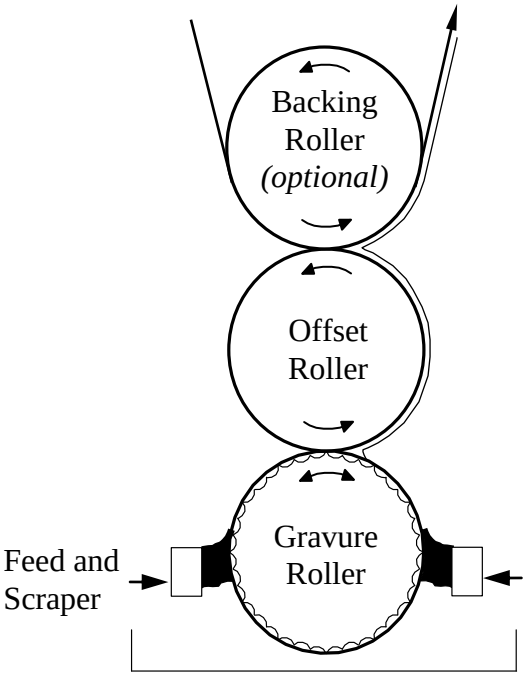

Offset, forward or reverse

Fig. 2

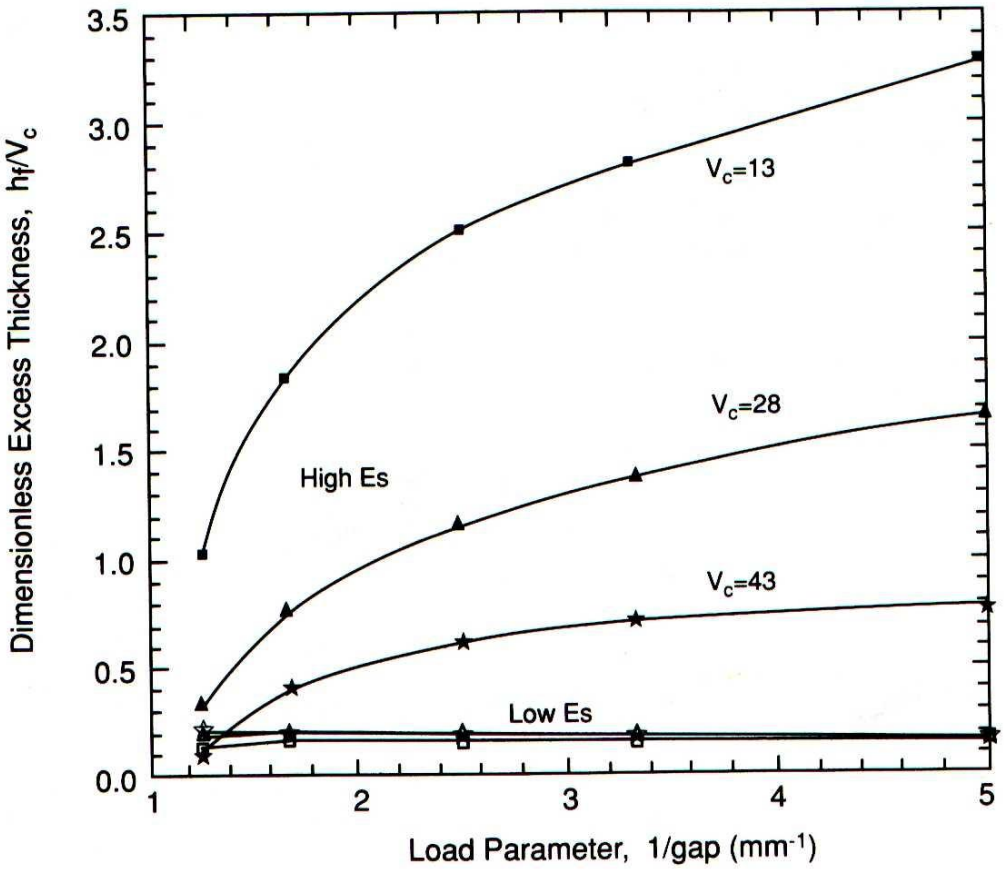
Dimensionless Excess Thickness, h_f/V_c
3.5
3.0
2.5
2.0
1.5
1.0
0.5
0.0
1
2
3
4
5
Load Parameter, 1/gap (mm^{-1})
V_c=13
V_c=28
V_c=43
High Es
Low Es

Fig 3

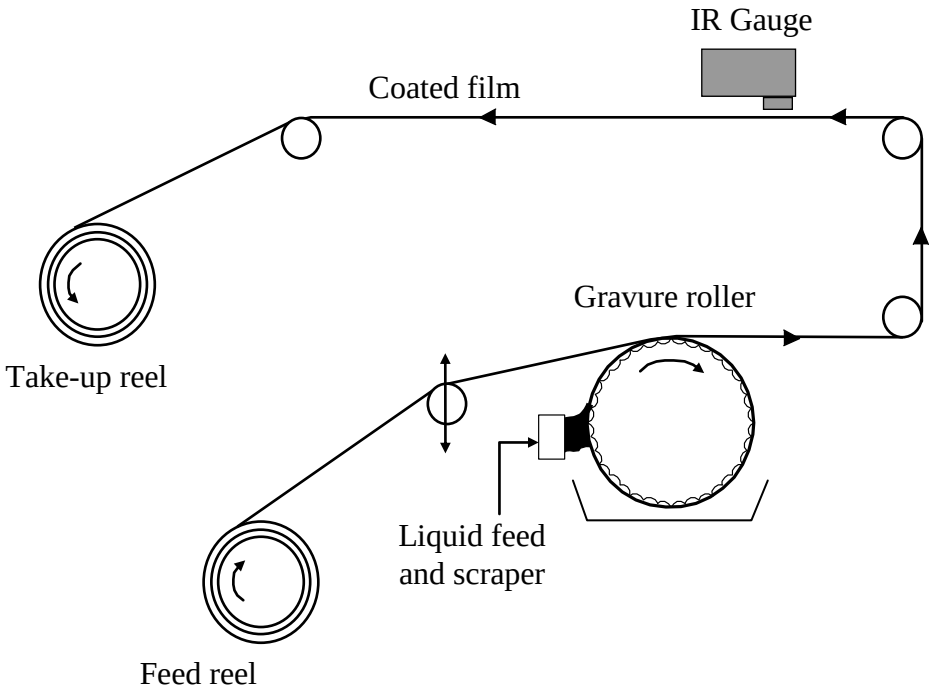
IR Gauge
Coated film
Gravure roller
Take-up reel
Liquid feed
and scraper
Feed reel

Fig. 4

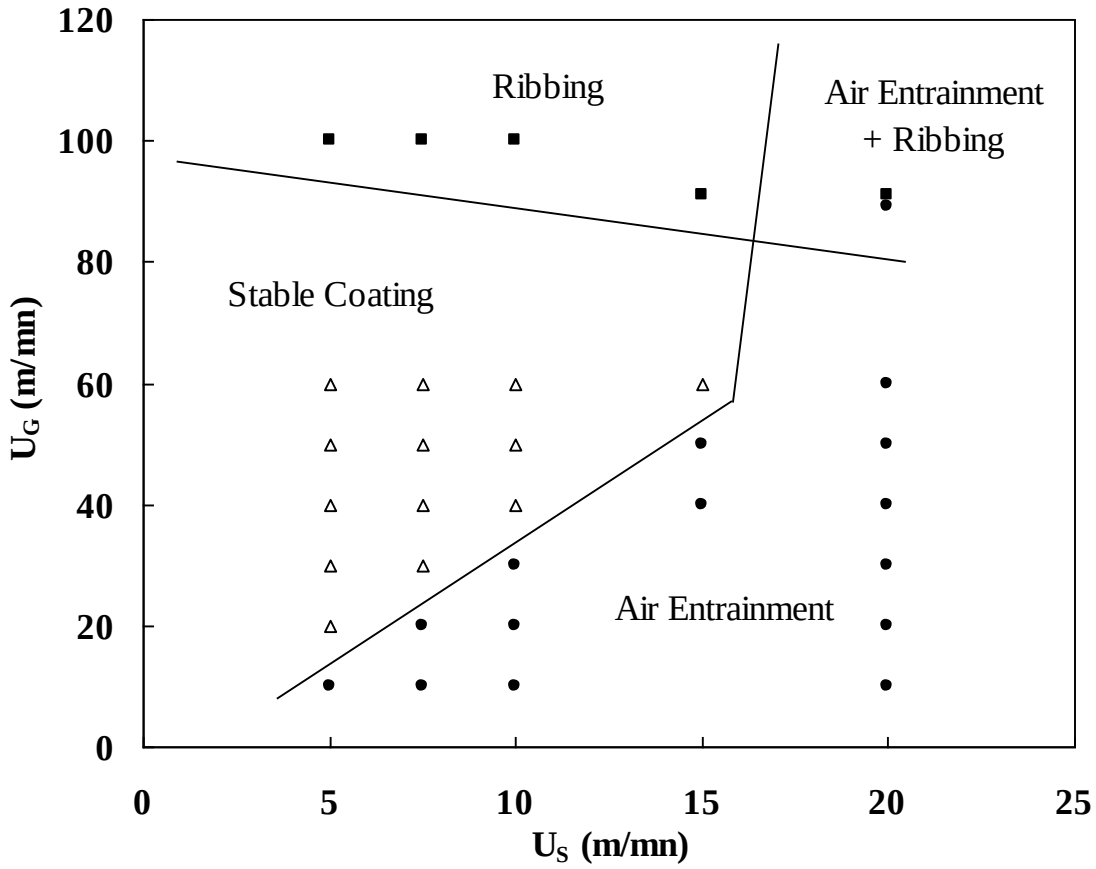
120
100
80
60
40
20
0
U_G (m/mn)
Ribbing
Air Entrainment
+ Ribbing
Stable Coating
Air Entrainment
0
5
10
15
20
25
U_S (m/mn)

Fig. 5

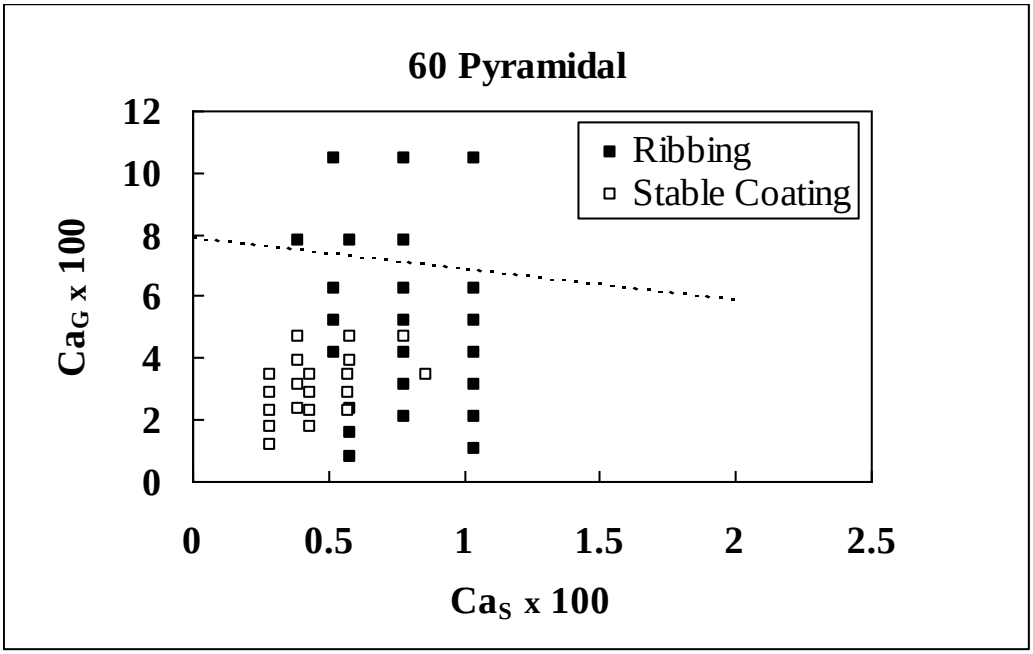
60 Pyramidal
Ribbing
Stable Coating
Ca_G x 100
Ca_S x 100
0
2
4
6
8
10
12
0
0.5
1
1.5
2
2.5

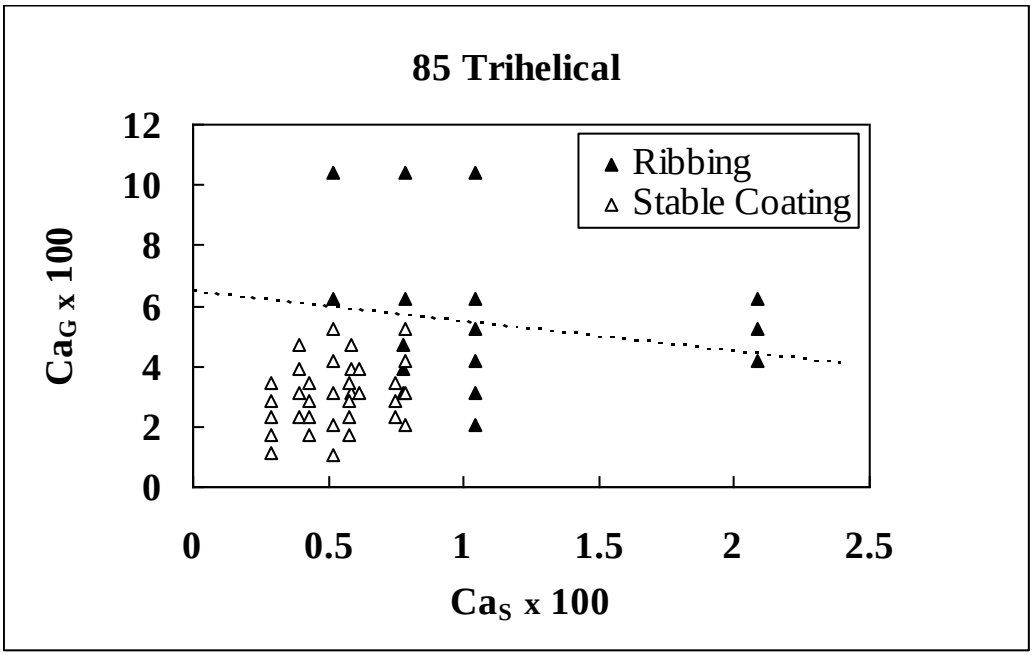
85 Trihelical
Ribbing
Stable Coating
Ca_G x 100
Ca_S x 100
0
2
4
6
8
10
12
0
0.5
1
1.5
2
2.5

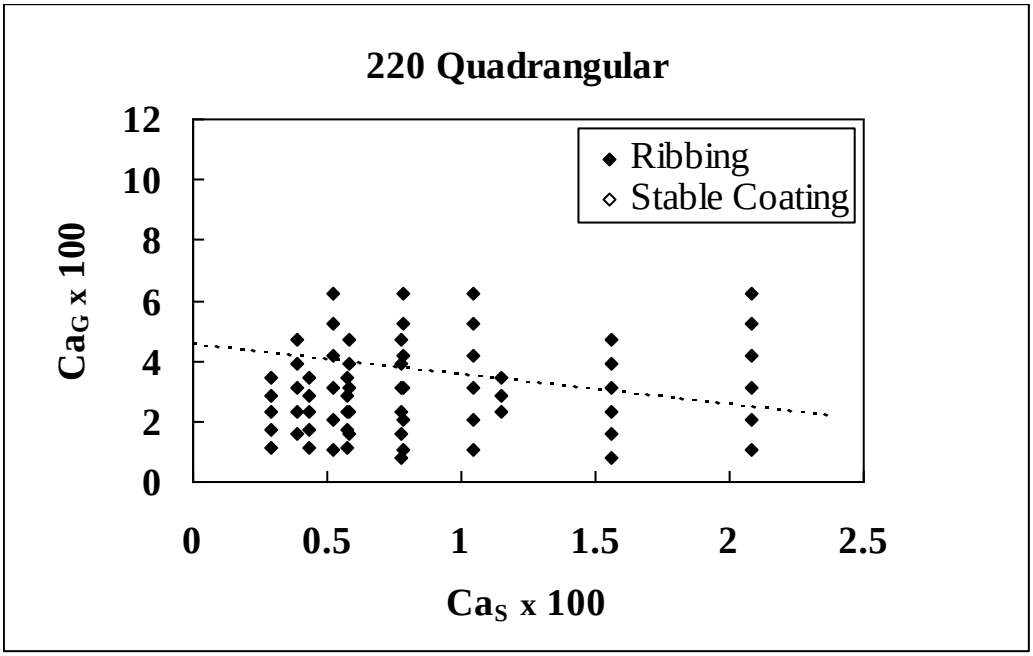

above figures are Fig.6
figure below is fig.7

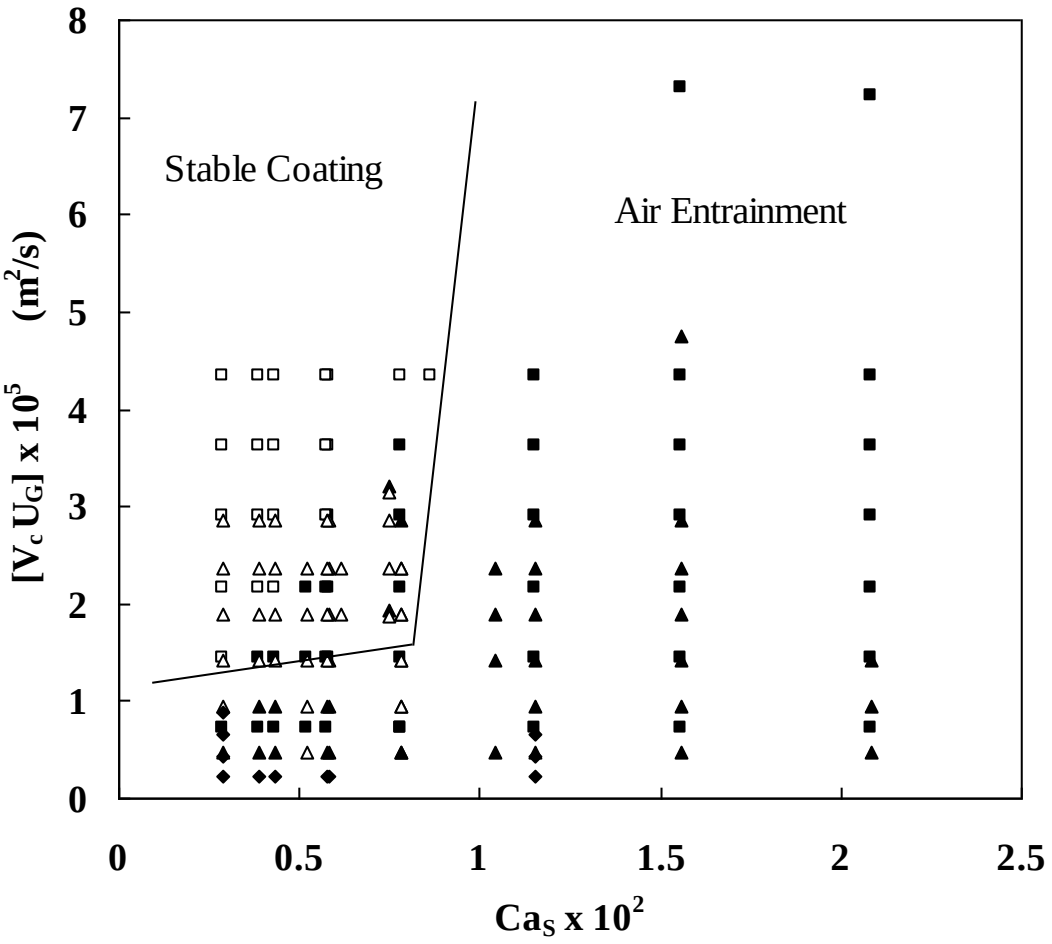
Stable Coating
Air Entrainment
[V_c U_G] x 10^5 (m^2/s)
Ca_S x 10^2
0
1
2
3
4
5
6
7
8
0
0.5
1
1.5
2
2.5

Fig. 7

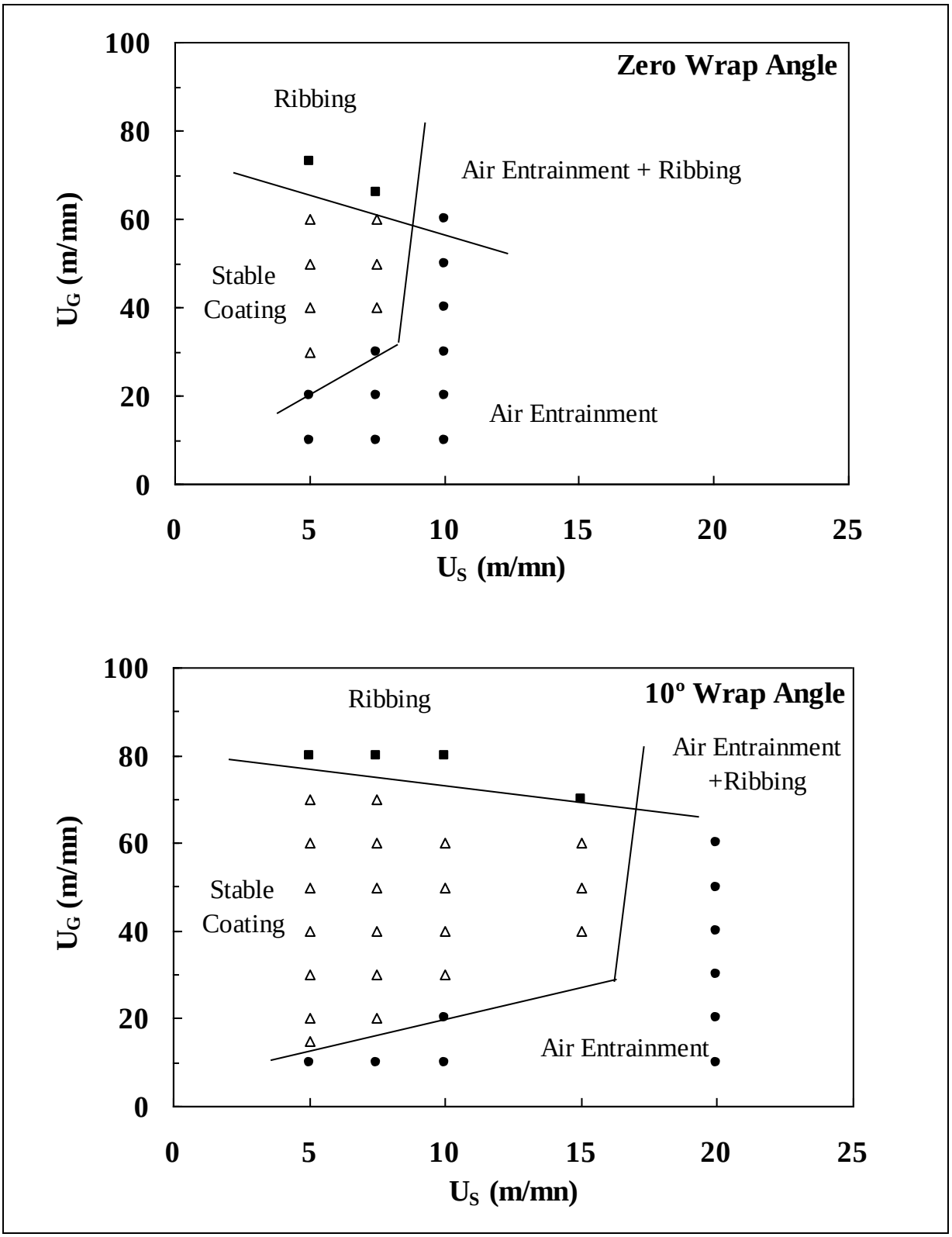
Zero Wrap Angle
Ribbing
Air Entrainment + Ribbing
Stable Coating
Air Entrainment
U_G (m/mn)
U_S (m/mn)
0
20
40
60
80
100
0
5
10
15
20
25
10º Wrap Angle
Ribbing
Air Entrainment +Ribbing
Stable Coating
Air Entrainment
U_G (m/mn)
U_S (m/mn)

Fig. 8

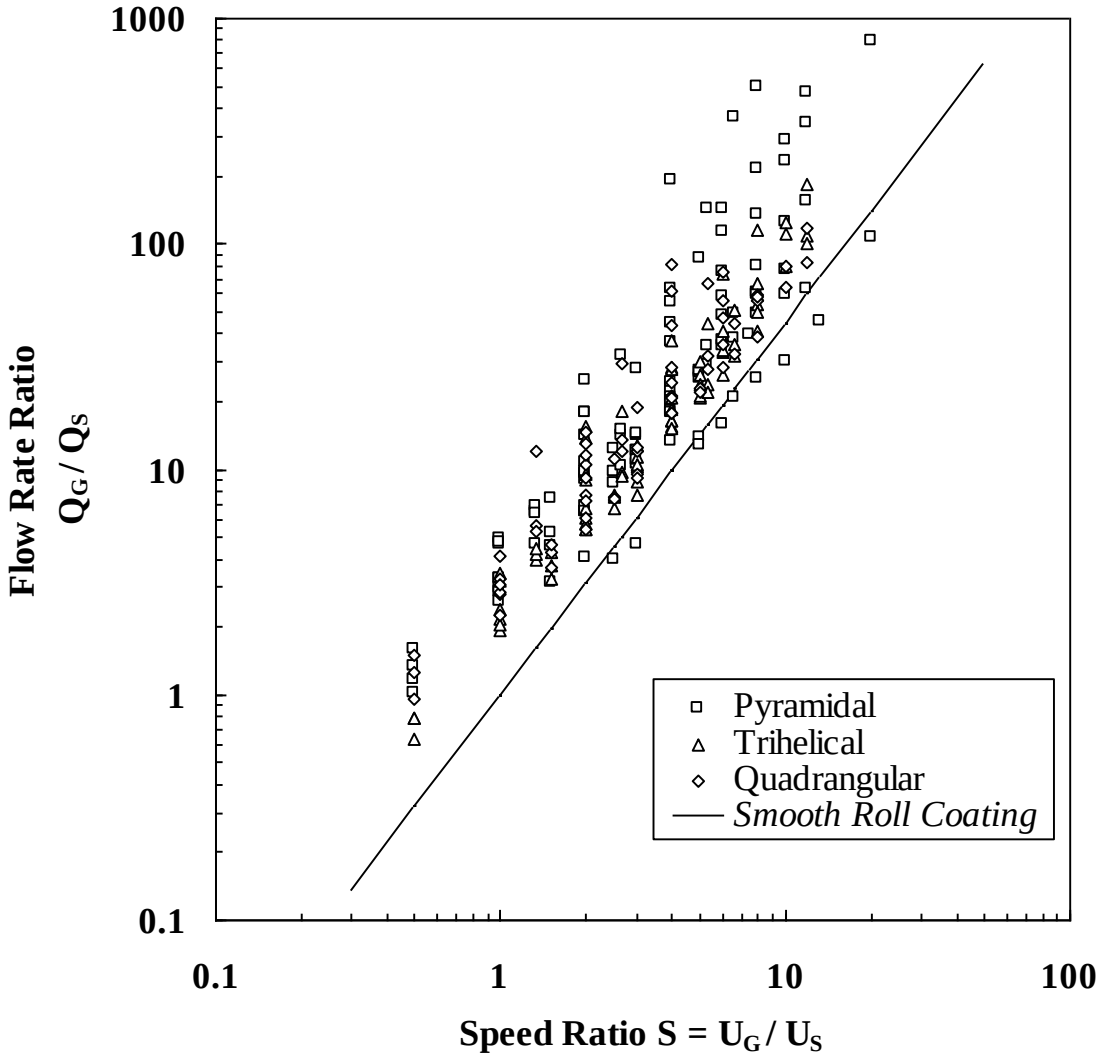
1000
100
10
1
0.1
Flow Rate Ratio
Q_G / Q_S
0.1
1
10
100
Speed Ratio $S = U_G / U_S$
Pyramidal
Trihelical
Quadrangular
Smooth Roll Coating

Fig. 9

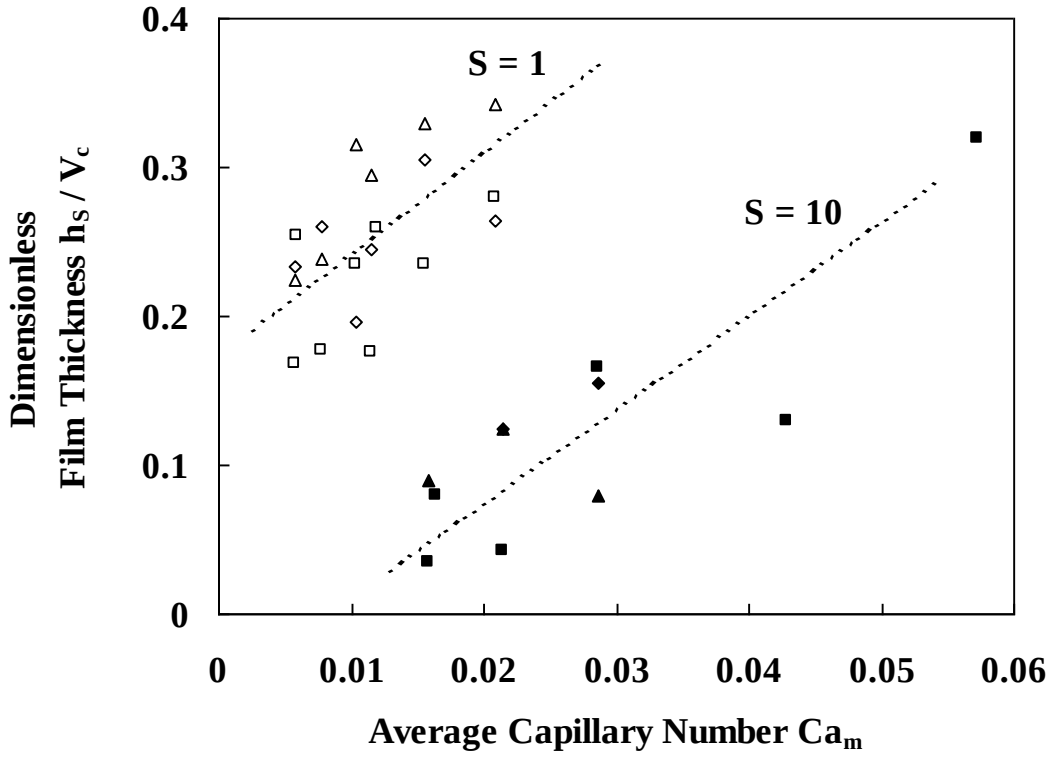
0.4
0.3
0.2
0.1
0
S = 1
S = 10
Dimensionless
Film Thickness h_S / V_c
0
0.01
0.02
0.03
0.04
0.05
0.06
Average Capillary Number Ca_m

Fig. 10